J Appl Electrochem (2009) 39:2073–2081
DOI 10.1007/s10800-009-9866-6

ORIGINAL PAPER

# From ceria nanotubes to nanowires through electrogeneration of base

P. Bocchetta · M. Santamaria · F. Di Quarto

Received: 7 October 2008 / Accepted: 5 March 2009 / Published online: 18 March 2009


**Abstract** The preparation of $Ce(OH)_3/CeO_2$ nanostructures (NSs) through electrogeneration of base into anodic alumina membranes was studied. The effects of solvent (alcohol and/or water), $Ce^{3+}$ partner anion nature (chloride or nitrate) and concentration, applied potential or current density in driving the morphology toward nanowires (NWs) and/or nanotubes (NTs) was described. The structural analysis performed by X-Ray Diffraction and Raman Spectroscopy allowed to evidence that the presence of Ce(IV) into the nanostructures strongly depends on the oxygen content in the growing environment.

**Keywords** Ceria · Nanowires · Nanotubes · Template · Electrogeneration of base

## 1 Introduction

In recent years electrodeposition of several metal hydroxides and oxides has been successfully achieved at room temperature by electrogeneration of base from the cathodic reduction of metal salt solutions such as nitrate or chloride [1–4]. Oxide can be directly produced via electrogeneration of base from properly selected organic solvent or indirectly by thermal treating the corresponding hydroxide. This technique has been recently adapted as a soft electrochemical route to the preparation of nanotubes/nanowires metal hydroxides and/or oxides through the employment of a template [5–9]. The deposition of metal hydroxides involves two steps at the cathode/electrolyte interface: the cathodic generation of hydroxyl ions and the chemical precipitation of the hydroxide. Both steps depend on the nature of chemical species present in the electrolyte subjected to the reduction process as well as on the local concentrations and solubility product of the hydroxide/oxide in the employed solvent. Owing to presence of an electric field, the electrolytic deposition allows better control of the deposition rate and deposit uniformity, also on substrates of complex shape such as anodic alumina membrane (AAM). Only few examples are reported in the literature on the effect of different parameters in controlling the morphologies of the nanostructures inside a hard template, and are mainly related to metal deposition. For instance, the pulse voltage during the electrodeposition into track-etched polycarbonate membrane has been used to pass from Co and Fe nanowires to nanotubes [10] and the template pore-wall-modification method has been recently developed [11–14] to fabricate metal nanotubes array using a porous alumina film.

To the best of our knowledge nothing is reported in the literature about the possibility to control, during electrodeposition inside AAM, the shape of the oxide and/or hydroxide nanostructures (NSs), which in turn considerably influences the practical applications. For instance, owing to their hollow interiors and high specific area, ceria nanotubes find applications as auto exhaust catalysts [15–17] and/or as co-catalysts for enhancing the performances in terms of higher thermal stability and catalytic activity [18–23], while $CeO_2$ nanowires can be employed as oxygen sensor [24], for energy storage [25] and as electrolyte for intermediate temperature solid oxide fuel cell (IT-SOFC) [26, 27]. This last potential application is really promising considering that doped ceria has been investigated over the past 20 years as possible oxide-ion electrolyte competitive with stabilized zirconia [26, 28–34] with the advantages of

P. Bocchetta (✉) · M. Santamaria · F. Di Quarto
Dipartimento di Ingegneria Chimica dei Processi e dei Materiali, Università di Palermo, Viale delle Scienze, 90129 Palermo, Italy
e-mail: bocchetta@dicpm.unipa.it

higher ionic conductivity at lower operation temperature (700–800 °C vs. 900–1,000 °C currently used for zirconia-based electrolyte). On the other hand, if we take into account that AAMs have been proved to be efficient support of ionic conductor in low temperature fuel cells [9, 35–37], allowing to decrease the ionic conductor thickness in absence of short circuits and gas crossover, the possibility to directly use the AAM/NWs composite in thin film fuel cell appears really appealing.

In a previous work [8] we have shown that high quality arrays of $Ce(OH)_3/CeO_2$ nanotubes can be prepared via electrogeneration of base into AAM pores from a cerium nitrate aqueous solution, while the same process carried out in ethanol solution containing cerium chloride brings to the formation of nanowires structures [9]. Starting from these findings, in this work we exploit the possibility to design a process, i.e. template-assisted electrogeneration of base, toward the formation of NTs or NWs for specific applications. At this aim the influence of different electrodeposition parameters on the morphology of the grown $Ce(OH)_3/CeO_2$ nanostructures without any pre-treatment of alumina template is examined. The effects of solvent (alcohol and/or water), nature (chloride or nitrate) and concentration of $Ce^{3+}$ partner anion, applied potential or current density in driving the morphology toward nanowires and/or nanotubes are described.

## 2 Experimental

### 2.1 Synthesis of $Ce(OH)_3/CeO_2$ nanostructures

Commercial anodic alumina membranes (Whatman, average pore diameter 200 nm, porosity 43%) were employed as template. Gold was sputtered on one side of the membrane to serve as conductive layer. AAM/Au electrodes were electrically connected with aluminum using a silver paste. The active surface area exposed to the solution was delimited by using 1) a holder with silicon gaskets, 2.54 $cm^2$ and 2) an insulating lacquer (Lacomit, UK) 1 $cm^2$. The AAM/Au electrodes were left in the electrolyte for 2 h before the electrodeposition in order to allow the permeation of solution within the membrane pores.

The electrodeposition process was carried out by using multichannel potentiostat VMP2 (Princeton Applied Research) in both aqueous and non aqueous (in ethanol) solution. $CeCl_3 \cdot 7H_2O$ or $Ce(NO_3)_3 \cdot 6H_2O$ were employed as solute for the deposition of $Ce(OH)_3/CeO_2$ NSs, and $Co(NO_3)_2 \cdot 6H_2O$ was added in order to prepare cerium-cobalt containing NWs.

A classic three-electrode cell was employed with the AAM/Au as working electrode, a DSA (Dimensionally Stable Anode) as counter electrode and a saturated calomel electrode (SCE) as reference electrode. For ethanol containing solutions, the reference was connected with the cell through a salt bridge and the anodic and cathodic compartments were separated by a sintered glass disk.

Thermal treatment of AAM/NSs was realized in an oven at 500 °C in air.

### 2.2 Characterizations

Morphology and quality of the NSs were investigated by using a Philips XL30 ESEM Scanning Electron Microscope (SEM). The AAM/NSs samples were sometimes chemically etched in 1 M NaOH for 2 h in order to remove the alumina host, and successively washed in $H_2O$ and filtered, producing numerous pieces of random broken NSs arrays on the stub. Energy dispersive X-ray analysis (EDX) was also performed in order to identify the elements into the deposited materials. X-ray analysis of composite AAM/NSs arrays was realized by a Philips X-Ray Generator (Model PW 1130) and a PW (Model 1050) goniometry.

All diffractograms were obtained in the $2\theta$ range 10°–100° with a step of 0.02° and a measuring time of 0.5 s for step, using copper K$\alpha$ radiation ($\lambda = 1.54$ Å). The identification was performed according to the ICDD (The International Centre for Diffraction Data®) available cards.

Raman spectra were obtained at room temperature using a Renishaw (inVia Raman Microscope) spectrometer equipped with a microprobe (50x) and a CCD detector. The excitation was provided by the 532 nm line of a Nd:YAG laser. The power of the incident beam on the sample was 5 mW and the width of the analyzed spot for each sample was about 2 µm. The time of acquisition was adjusted according to the intensity of the Raman scattering. The wavenumber values reported in the spectra have 1 $cm^{-1}$ accuracy. The Raman analysis were performed in different areas of the the surface sample in order to verify the homogeneity of the deposit.

## 3 Results and discussion

In Fig. 1 we report the current vs time curves recorded during potentiostatic polarization of the AAM/Au electrodes in 0.3 M $CeCl_3 \cdot 7H_2O$ ethanol solution. In these conditions, uniform, continuous and high ordered network of nanowires form without an appreciable influence of the electrical conditions on their morphology, according to the SEM images of the nanostructures after AAM removal (see Fig. 2).

Under the applied cathodic potentials the circulating current can be sustained by the following reduction processes:

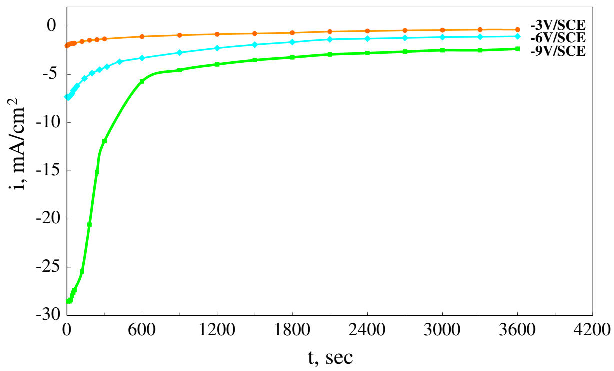


**Fig. 1** Current density vs. time during the electrodeposition of Ce oxy-hydroxide NWs inside porous AAM in 0.3 M $CeCl_3 \cdot 7H_2O$ in ethanol solution at different applied potentials: −9 V/SCE; −6 V/SCE; −3 V/SCE

$$2H_2O + 2e^- \rightarrow H_2 + 2OH^- \quad (1a)$$

$$2H_3O^+ + 2e^- \rightarrow H_2 + 2H_2O \quad (1b)$$

$$O_2 + 2H_2O + 4e^- \rightarrow 4OH^- \quad (1c)$$

$$O_2 + 2H_2O + 2e^- \rightarrow 2OH^- + H_2O_2 \quad (1d)$$

According to the following equation, the reduction of solvent cannot be excluded [38] owing to the high cathodic potential applied during the deposition,:

$$CH_3CH_2OH + 3H_2O + 4e^- \rightarrow 2CH_4 + 4OH^- \quad (1e)$$

All these half-cell reactions produce under cathodic polarization a pH increase at the cathode (bottom of AAM), inducing the precipitation into the AAM pores of cerium hydroxides $Ce(OH)_3$ [39]:

$$Ce^{3+} + 3OH^- \rightarrow Ce(OH)_3\downarrow \quad (2a)$$

and/or the formation of Ce(IV) ionic species [40, 41]:

$$2Ce^{3+} + H_2O_2 + 2OH^- \rightarrow 2Ce(OH)_2{}^{2+} \quad (2b)$$

responsible of the precipitation of $CeO_2$ according to the following reaction:

$$Ce(OH)_2^{2+} + 2OH^- \rightarrow CeO_2 + 2H_2O \quad (3)$$

The reactions (1c), (2b) and (3) are less probable because of the great number of involved species and the very low oxygen concentration inside the pores, bringing to a low $CeO_2$ content into the deposited NSs. This suggestion is confirmed by the X-ray diffraction patterns of the composite AAM/NSs prepared by polarizing the AAM/Au electrodes, for 1 h at −3, −6 and −9 V/SCE, in 0.3 M $CeCl_3 \cdot 7H_2O$ ethanol solution (see Fig. 3). The AAM/NWs of Fig. 3 are mainly constituted of $Ce(OH)_3$ (ICCD 74-0665 card) with broad and not pronounced peak, due to the presence of the AAM host and/or to scarce cristallinity. The main peak at 28,8° relative to $CeO_2$ (ICCD 34-0394 and 81-0792) appears only when the circulated charge is enough to allow the complete pore filling and the subsequent formation of a compact layer over the AAM template, where more oxygen is available. This is the case of the electrodeposition performed at −9 V/SCE for 1 h,

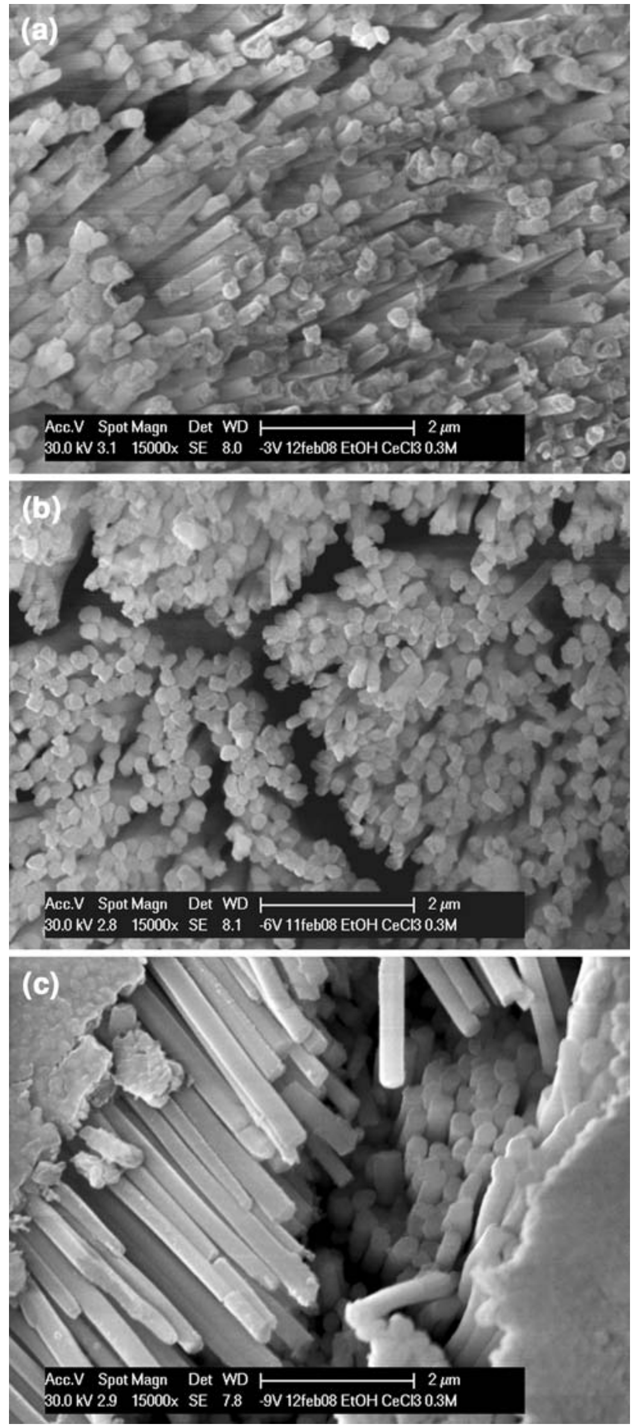


**Fig. 2** S.E.M. images of Ce oxy-hydroxide NWs after removal of the alumina template electrodeposited in 0.3 M $CeCl_3 \cdot 7H_2O$ ethanol solution for 1 h at different applied potentials. **a** −3 V/SCE; **b** −6 V/SCE; **c** −9 V/SCE

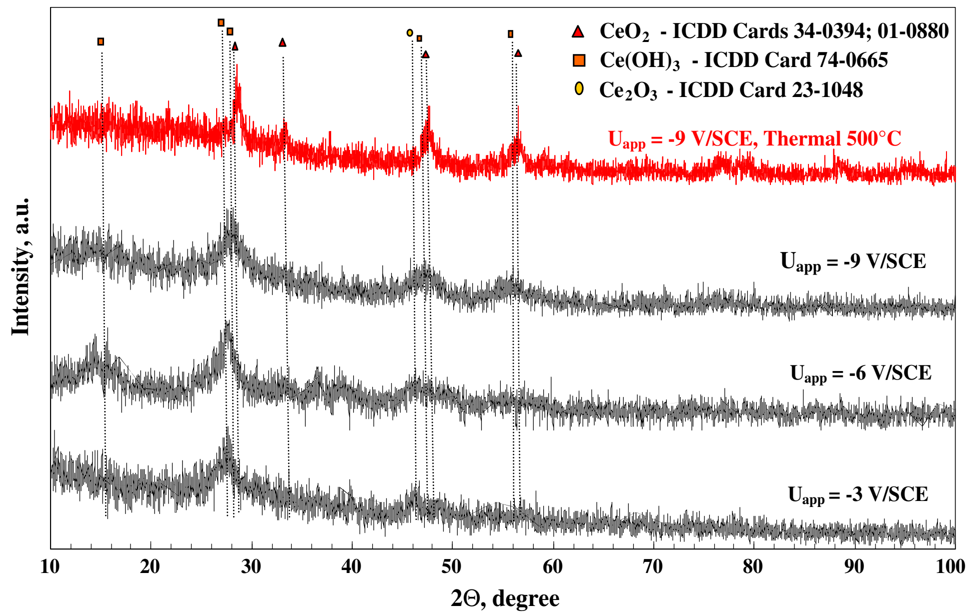


**Fig. 3** X-ray diffractograms of AAM/NWs prepared in 0.3 M $CeCl_3 \cdot 7H_2O$ ethanol solution at different applied potentials (−9 V/SCE; −6 V/SCE; −3 V/SCE) for 1 h. The thermal treatment of AAM/NWs prepared at −9 V/SCE has been performed at 500 °C for 4 h under air exposure

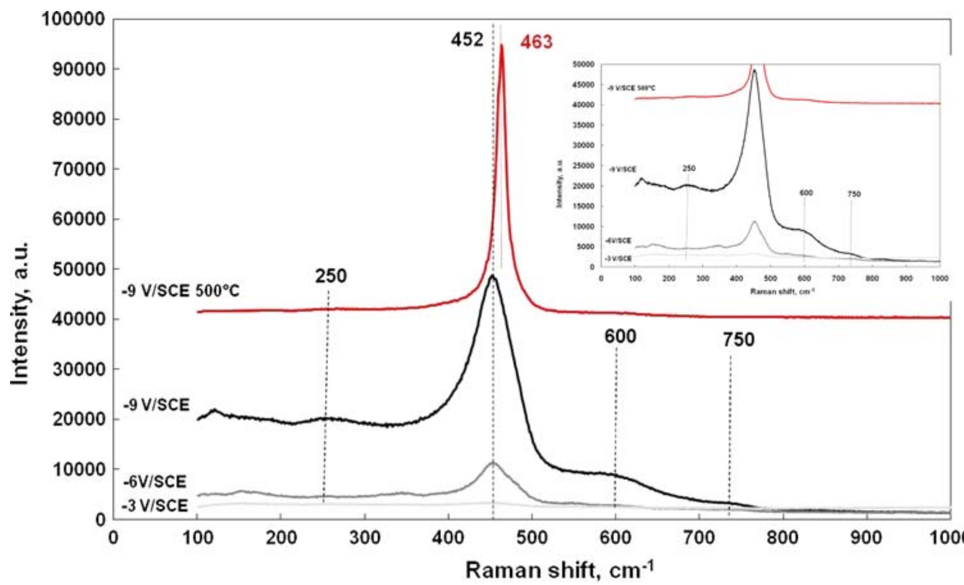


**Fig. 4** Raman spectra of AAM/NWs prepared in 0.3 M $CeCl_3 \cdot 7H_2O$ ethanol solution at different applied potentials (−9 V/SCE; −6 V/SCE; −3 V/SCE) for 1 h

where the presence of a compact layer 13 μm thick over the nanodeposit array was revealed. This finding was confirmed by comparing the XRD spectra relating to AAM/NWs assemblies prepared at the same current density for several circulating charges corresponding to partially filled and covered templates (see ref. 9), and is in agreement with XPS analysis performed on thin films electrodeposited from 0.3 M $CeCl_3 \cdot 7H_2O$ in naturally aerated ethanol solution [42].

According to the XRD spectra of Fig. 3, thermal treatments (4 h at 500 °C under air exposure) of AAM/NWs samples induce the complete oxidation of $Ce(OH)_3$ to $CeO_2$ and improve the crystallinity of the deposited materials.

The described results have been also confirmed by Micro Raman Spectroscopy analysis. The Raman spectra of AAM/NWs of Fig. 1 display bands at 250, 452, 600 and 750 $cm^{-1}$ (Fig. 4). The prominent band at 452 $cm^{-1}$ can be assigned to the symmetric breathing mode of O atoms around each $Ce^{4+}$ cation (Raman mode in metal dioxides with fluorite structure), while the weaker band at 250 $cm^{-1}$ can be referred to cubic $CeO_2$ second order scattering [43, 44]. The main line at 452 $cm^{-1}$ is in good agreement with the value of 454.2 $cm^{-1}$ reported in [45] for ceria films cathodically deposited on steel substrate from Ce(III) chloride solution, while it is sensibly different from the frequency of 466 $cm^{-1}$ often reported in the literature for single crystal $CeO_2$. The peak around 600 $cm^{-1}$ is usually assigned to the oxygen vacancies due to the nonstoichiometry of $CeO_2$ and often reported in literature for nanocrystalline ceria [46, 47]. In agreement with XRD results, the peaks intensity (related to $CeO_2$) performed on AAM/NWs samples decreases drastically with the applied potentials (or deposit thickness), due to the low percentage of $CeO_2$ lattice. The thermal treatment of AAM/$CeO_2$ samples (Fig. 4) induces a shift of the intense band from 452 to 463 $cm^{-1}$ together with a sharpening and an improved symmetry, attributed to the grain size of the sample increasing at higher calcination temperature (better crystallization) [48].

In conclusion, the use of ethanol and $CeCl_3 \cdot 7H_2O$ allows to prepare high quality $Ce(OH)_3/CeO_2$ NWs, which can be completely oxidized by thermal treatment to ceria NWs.

Since our recent results [8] have proved that also ceria NTs can be produced via electrogeneration of base by using an aqueous solution, we have evaluated the effect of water content on the morphology of the nanostructures. The addition of water into 0.3 M $CeCl_3 \cdot 7H_2O$ ethanol electrolyte brings to the formation of mixed arrays of nanowires and nanotubes, as shown in Fig. 5, where the morphologies of nanodeposits prepared in mixed ethanol/water solvent at different $H_2O$/EtOH ratios are reported. This indicates that the nanowire growth is the preferred process only when the water acts as solute, as in the case of $CeCl_3 \cdot 7H_2O$ in ethanol. Nanotubes morphology appears when water behaves like solvent, evidencing that the dielectric constant of the electrolyte and, thus, the solubility of the hydroxide/oxide in the employed solvent, is a key factor. This is confirmed also by electrodepositions performed using an amphiprotic solvent with dielectric constant close to that of ethanol, i.e. methanol, which produce nanowires arrays with morphologies very similar to those obtained in ethanol [9].

According to the literature [49], the addition of ethyl alcohol into an aqueous electrolyte promote particle coagulation and gel formation because reduces the solubility of the deposit. This procedure is commonly used in the corrosion field because leads to homogeneous and continuous coatings with reduced cracked areas and porosity [50]. Our results suggest that these features can be reported to a restricted geometry, such us the nanometric pores of AAMs, leading to a complete and uniform filling of the pore and, thus, to a nanowire morphology. This can be explained considering that hydrolysis reactions result in the accumulation of colloidal particles at the pore bottom (cathodic area) that form a deposit by flocculation assisted by the electrolyte (according to DLVO theory of colloidal stability [49]). Thus, a lower solubility of the hydroxide/oxide induces a more enhanced coagulation of colloidal particles near the cathode, because of the high concentration and pressure resulting from the formation of new particles.

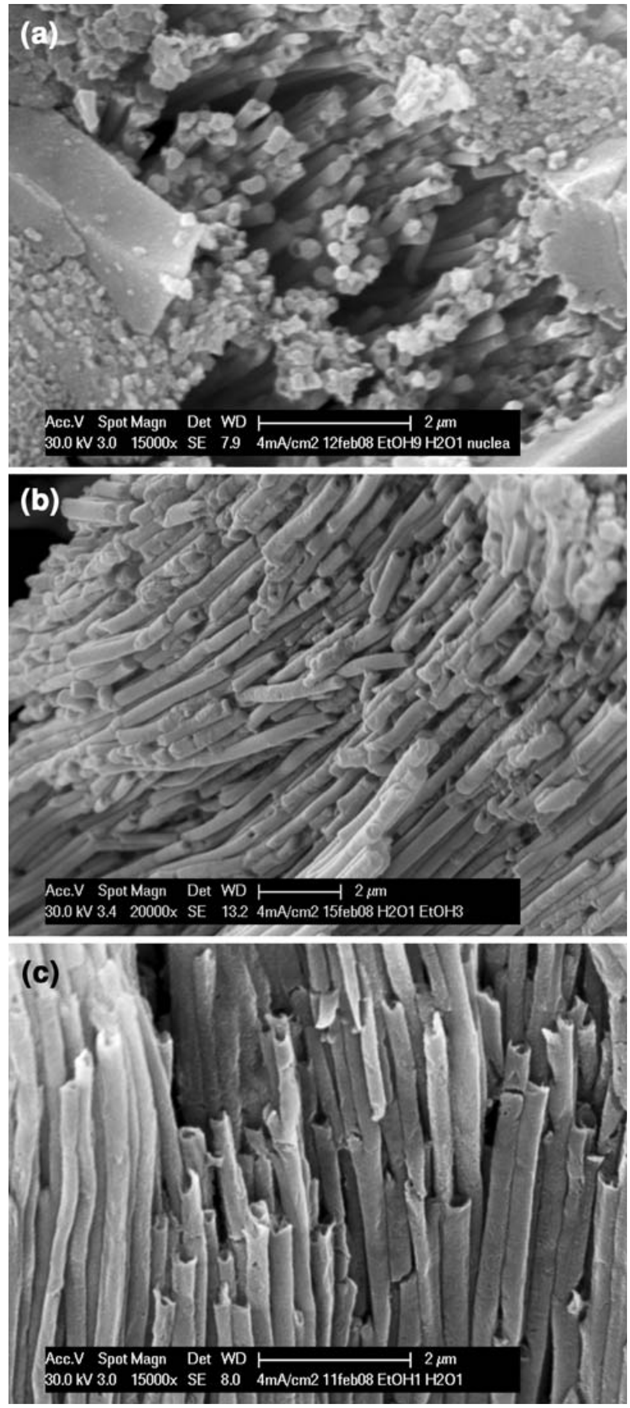


**Fig. 5** S.E.M. images of Ce oxy-hydroxide nanostructures after removal of the alumina template electrodeposited in 0.3 M $CeCl_3 \cdot 7H_2O$ ethanol solution at i = 4 mA/$cm^2$ for 1 h at different $H_2O$/EtOH ratios. **a** $H_2O$/EtOH = 10% vol; **b** $H_2O$/EtOH = 25% vol; $H_2O$/EtOH = 50% vol

The synergetic *wiring* effect of chloride/ethanol was successfully employed for preparation of mixed Ce/Co

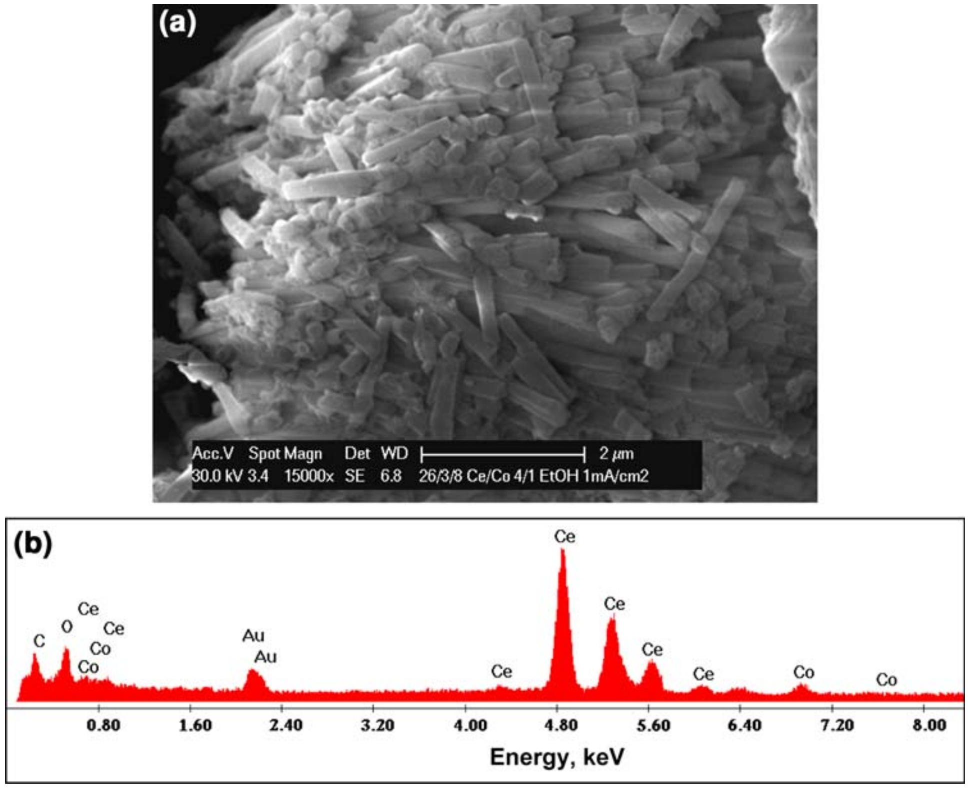


**Fig. 6** **a** S.E.M. image of Ce/Co oxy-hydroxide NWs after removal of the alumina template electrodeposited in 0.24 M $CeCl_3 \cdot 7H_2O$ + 0.06 M $Co(NO_3)_2$ $7H_2O$ ethanol solution at $i = 4$ mA/cm$^2$ for 1 h. **b** Energy-dispersive X-ray (EDX) spectrum corresponding to the specimens of Fig. 6a

oxi-hydroxide nanowires through electrogeneration of base into AAM. In Fig. 6 we report the SEM image of the nanostructure after AAM removal deposited from a $CeCl_3 \cdot 7H_2O/Co(NO_3)_2$ $7H_2O$ in ethanol solution. A nanowire-type morphology is evident, while energy-dispersive X-ray (EDX) spectrum (corresponding to the specimens in Fig. 6a) reveals the Ce and Co peaks, indicating the co-deposition of cerium and cobalt. If we consider that the addition of small amount of cobalt oxide to gadolinia-stabilized ceria resulted in much lower sintering temperature, higher shrinkage rates and grain sizes in the final sintered product [51–54], these preliminary results appear promising for SOFC electrolyte applications.

The current results obtained in $CeCl_3 \cdot 7H_2O$ mixed water/ethanol solvent emphasized that water exhibits a significant *tubizing* effect on the morphological growth of the hydroxide, but neither the employment of pure water solvent is enough to produce uniform and high quality $Ce(OH)_3$ nanotubes, as shown in Fig. 7.

In order to check a possible influence of solute concentration we also performed electrogeneration of base process in more dilute solution. As shown in Fig. 8a the morphology of the nanostructures prepared in 0.05 M cerium chloride in water is very similar to that obtained in more concentrate electrolytes.

As already found in alcoholic solution, the morphological features of nanostructures deposited in aqueous solution are almost independent on the electrical parameters as confirmed by the SEM analysis relating to nanostructures prepared in a wide current density range. From 4 mA cm$^{-2}$ down to 10 µA cm$^{-2}$ (see Fig. 8b) the nanostructures maintain similar morphologies, consisting of mixed nanotubes/nanowires arrays.

In order to achieve high quality nanotubes arrays the metal chloride must be replaced with metal nitrate. Fig. 9 shows the SEM images of the $Ce(OH)_3/CeO_2$ nanotubes electrodeposited from 0.05 and 0.3 M $Ce(NO_3)_3 \cdot 6\,H_2O$ aqueous solution. In presence of cerium nitrate water solution, a further reduction process must be added to the eq. (1):

$$NO_3^- + H_2O + 2e^- \rightarrow NO_2^- + 2OH^- \qquad (4)$$

This reaction, which is thermodynamically favoured with respect to water reduction due to the high standard reduction potential of nitrate ions in aqueous solution, leads also to the $OH^-$ formation and, thus, to the subsequent hydroxide precipitation. According to the morphological findings, uniform arrays of hollow interior nanostructures can be produced only in absence of both ethanol and chloride ions, thus confirming that the kinetic of the coagulation of colloidal particles near the cathode is influenced also by $Cl^-$ ions, as already observed on flat geometry for ceria thin film, which are more adherent and uniform if prepared from $CeCl_3$ solutions with respect to other salts [55].

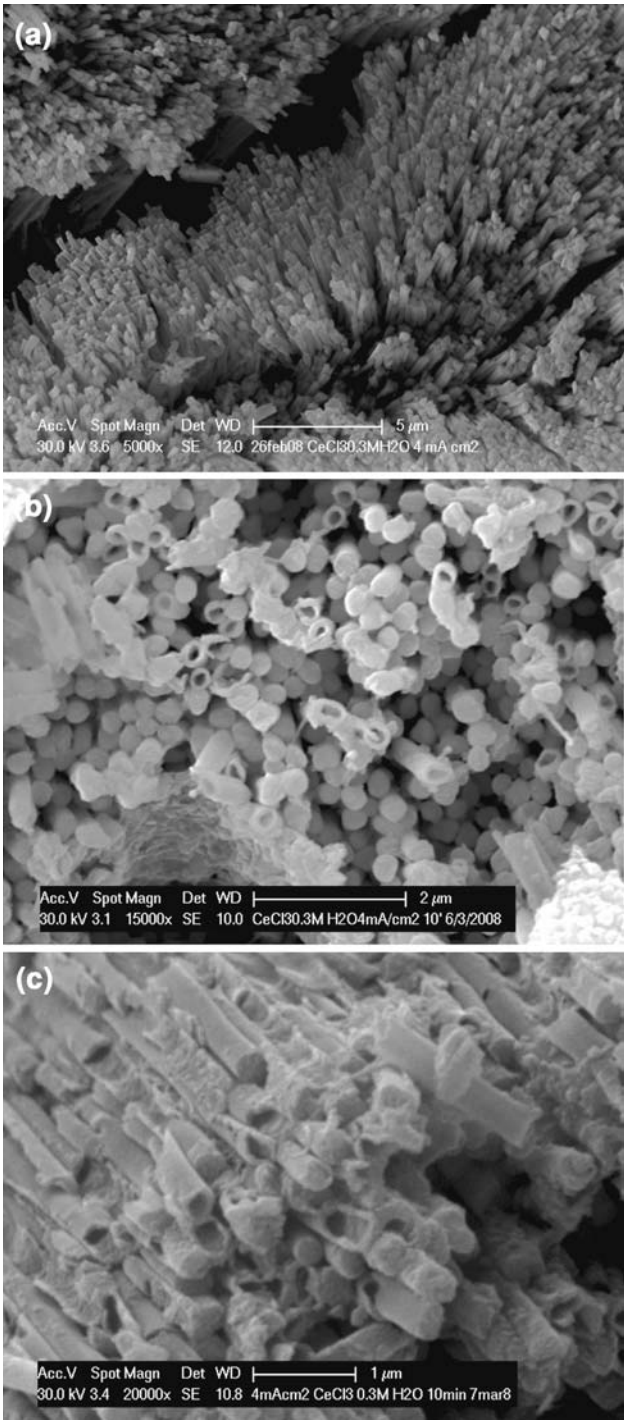


**Fig. 7** S.E.M. images at different magnifications of Ce oxy-hydroxide nanostructures after removal of the alumina template electrodeposited in 0.3 M $CeCl_3 \cdot 7H_2O$ aqueous solution at $i = 4$ mA/cm$^2$ for 1 h

In summary, the results obtained in aqueous baths indicate that the morphology cannot be precisely controlled by electrical parameters and the use of $Ce(NO_3)_3 \cdot 6\ H_2O$ remains the preferable way to make uniform and parallel cerium oxide nanotubes.

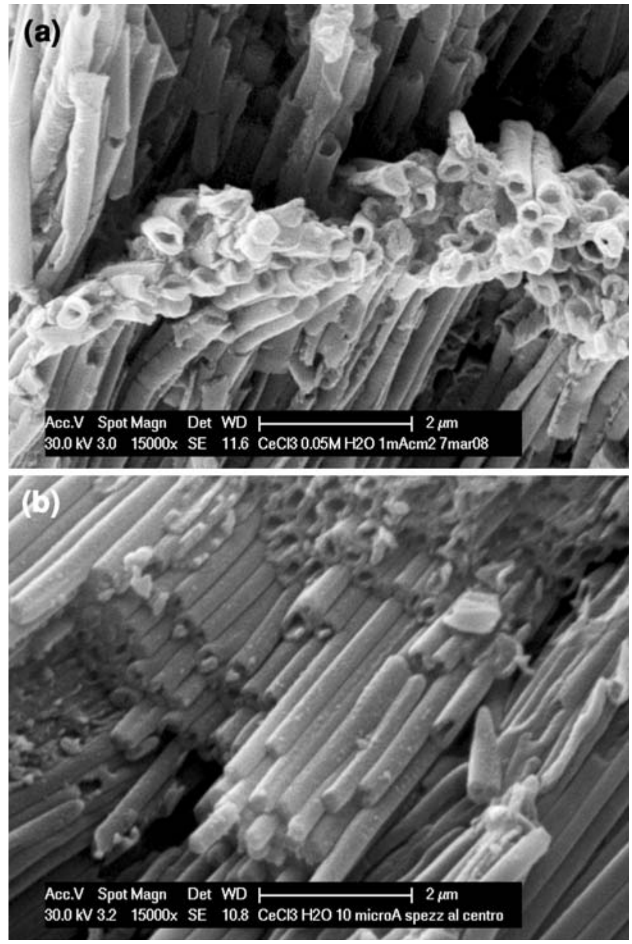


**Fig. 8** S.E.M. morphologies of Ce oxy-hydroxide nanostructures after removal of the alumina template electrodeposited in aqueous solution for 1 h. **a** 0.05 M $CeCl_3 \cdot 7H_2O$ at $i = 4$ mA/cm$^2$ and **b** 0.3 M $CeCl_3 \cdot 7H_2O$ at $i = 10$ μA/cm$^2$

## 4 Conclusions

The fabrication of cerium hydroxide/oxide nanowires and/or nanotubes via template-assisted electrogeneration of base has been investigated. The growth of the nanostructures was associated to the to the precipitation of $Ce(OH)_3$ induced by the pH increase on the cathode surface caused by the reduction processes, as well as to precipitation of $CeO_2$ induced by the formation of $Ce(OH)_2^{2+}$ complexes.

The experimental results suggest that there is not a strong influence of the electrical variables (i.e. current density or applied potential) in determining the morphology of the grown nanostructures, while their shape (nanowire or nanotube) can be controlled by an appropriate choice of anion and solvent. As general trend, it can be concluded that while water solvent and nitrate drive the deposits toward a nanotube morphology, ethanol and chloride drive the morphology of the deposit toward nanowires.

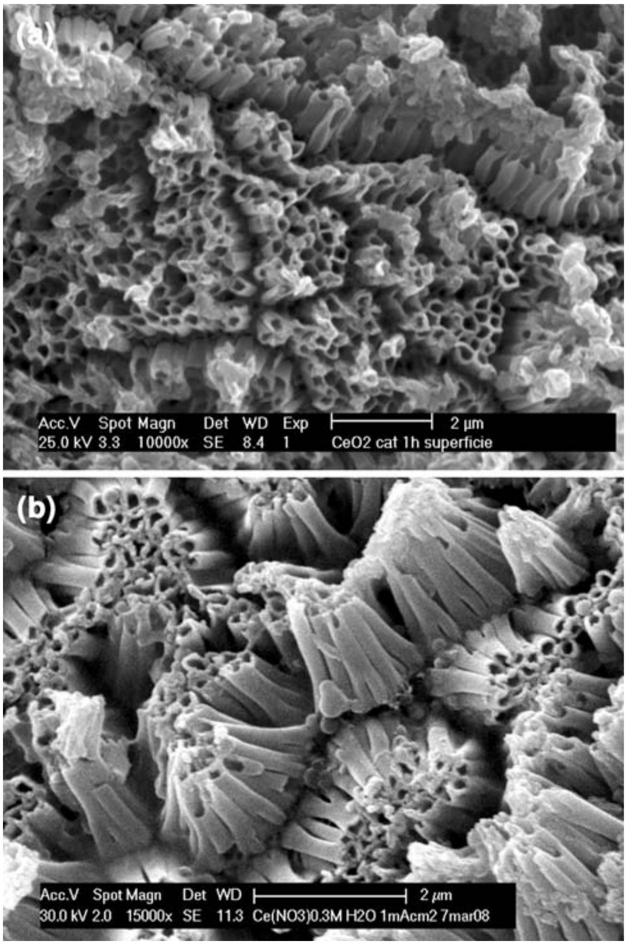


**Fig. 9** Surface morphology of free standing Ce oxy-hydroxide NTs after removal of the alumina template electrodeposited at $i = 1$ mA/cm$^2$ for 1 h in **a** 0.05 M in $Ce(NO_3)_3 \cdot 6\ H_2O$ and **b** 0.3 M in $Ce(NO_3)_3 \cdot 6\ H_2O$ aqueous solutions

As confirmed by XRD and Raman analyses, the structural features of the nanowires are influenced by the circulating charge but thermal treatments allowing the formation of $CeO_2$ (fluorite structure) via a complete oxidation of Ce(III) to Ce(IV) are necessary to enhance the crystallinity of the deposit.

In response to a growing need for metal-oxide nanotubes and nanowires for different applications, the template electrogeneration of base approach appears an efficient technique in fabricating nanowires and/or nanotubes. We are currently exploring the possibility to apply this method to other metal hydroxides/oxides in different nanometric shapes through the regulation of operational parameters.

**Acknowledgments** This work is sponsored by USAITC-A under contract N. W911NF-07-1-0564 and University of Palermo.

## References

1. Therese GHA, Kamath PV (2000) Chem Mater 12:1195
2. Nobial M, Devos O, Mattos OR, Tribollet B (2007) J Electroanal Chem 600:87
3. Therese HAG, Dinamani M, Kamath PV (2005) J Applied Electrochem 35:459
4. Yogeeswaran G, Chenthamarakshan CR, Seshadri A, De Tacconi NR, Rajeshwar K (2006) Thin Solid Films 515:2464
5. Lai M, Gonzalez Martinez JA, Grätzel M, Riley DJ (2006) J Mater Chem 18:2843
6. Oh J, Tak Y, Lee J (2004) Electrochem. Solid-State Lett 7:C2
7. Bocchetta P, Santamaria M, Di Quarto F (2007) Electrochem Comm 9:683
8. Bocchetta P, Santamaria M, Di Quarto F (2008) Electrochem Solid-State Lett 11:K27
9. Bocchetta P, Santamaria M, Di Quarto F (2008) Electrochem Solid-State Lett 9:K93
10. Tourillon G, Pontonnier L, Levy JP, Langlais V (2000) Electrochem Solid-State Lett 3:20
11. Brumlik CJ, Martin CR (1991) J Am Chem Soc 113:3174
12. Bao J, Tie C, Xu Z, Zhou Q, Shen D, Ma Q (2001) Adv Mater 21:13
13. Bao J, Xu Z, Hong J et al (2004) Scr Mater 50:19
14. Maschmann MR, Franklin AD, Amama PB, Zakharov DN, Stach EA, Sands TD, Fisher TS (2006) Nanotechnology 17:3925
15. Trovarelli A (1996) Catal Rev Sci Eng 38:439
16. Dictor R, Roberts S (1989) J Phys Chem 93:5846
17. Su EC, Rothschild WG (1986) J Catal 99:506
18. Kirchnerova J, Alifanti M, Delmon B (2002) Applied Catal A 231:65
19. Kang M, Song MW, Lee CH (2003) Applied Catal A 251:143
20. Natile MM, Glisenti A (2005) Chem Mater 17:3403
21. Lotta LF, Di Carlo G, Pantaleo G, Venezia AM, Deganello G (2006) Applied Catal B 66:217
22. Tang C-W, Kuo C-C, Kuo M-C, Wang C-B, Chien S-H (2006) Applied Catal A 309:37
23. Lotta LF, Di Carlo G, Pantaleo G, Deganello G (2007) Applied Catal B 70:314
24. Izu N, Shin W, Murayarna N, Kanzaki S (2002) Sens Actuators B87:95
25. Xiong Y, Yamaji K, Sakai N, Negishi H, Horita T, Yokokawa H (2001) J Electrochem Soc 148:E489
26. Steele BCH (2000) Solid State Ionics 129:95
27. Hormes J, Pantelouris M, Balazs GB, Rambabu B (2000) Solid State Ionics 136–137:954
28. Riley B (1990) J Power Sources 29:223
29. Educhi K, Setoguchi T, Inoue T, Arai H (1992) Solid State Ionics 52:165
30. Yahiro H, Baba Y, Eguchi K, Arai H (1988) J Electrochem Soc 135:2077
31. Minh NQ (1993) J Am Ceram Soc 76:563
32. Gödickemeier M, Gauckler LJ (1998) J Electrochem Soc 145:414
33. Gauckler LJ, Beckel D, Buergler BE, Jud E, Muecke UP, Prestat M, Rupp JLM, Richter J (2004) Chimia 58:837
34. Kharton VV, Figueiredo FM, Navarro L, Naumovich EN, Kovalevsky AV, Yaremchenko AA, Viskup AP, Carneiro A, Marques FMB, Frade JR (2001) J Mat Sci 36:1105
35. Bocchetta P, Chiavarotti GP, Masi R, Sunseri C, Di Quarto F (2004) Electrochem Comm 6:923
36. Bocchetta P, Conciauro F, Di Quarto F (2007) J Solid State Electrochem 11:1253
37. Bocchetta P, Ferraro R, Di Quarto F (2009) J Power Sources 187:49

38. Schmidt VM, Ianniello R, Pastor E, Gonzáles S (1996) J Phys Chem 100:17901
39. Böhm S, Greef R, McMurray HN, Powell SM, Worsley DA (2000) J Electrochem Soc 147:3286
40. Aldykiewicz AJ, Davenport AJ, Isaacs HS (1996) J Electrochem Soc 143:147
41. Li FB, Thompson GEJ (1999) Electrochem Soc 146:1809
42. Stefanov P, Atanasova G, Stoychev D, Marinova T (2004) Surf Coat Technol 180:446
43. Spanier JE, Robinson RD, Zheng F, Chan SW, Herman IP (2001) Phys Rev B: Condens Matter 64:2454
44. Weber WH, Hass KC, McBride JR (1993) Phys Rev B: Condens Matter 48:178
45. Creus J, Brezault F, Rebere C, Gadouleau M (2006) Surf Coat Technol 200:4636
46. Reddy BM (2002) J Phys Chem B 106:10964
47. McBride JR, Hass KC, Poinexter BD, Weber WH (1994) Appl Phys 76:2435
48. Kosacki I, Suzuki T, Anderson HU, Colomban P (2002) Solid State Ionics 149:99
49. Zhitomirsky I (2002) Adv Colloid Interface Sci 97:279
50. Zhitomirsky I, Petric A (2001) Ceram Int 27:149
51. Fagg DP, Kharton VV, Frade JR (2002) J Electroceram 9:199
52. Jud E, Zhang Z, Sigle W, Gauckler LJ (2006) J Electroceram 16:191
53. Jud E, Gauckler L, Halim L, Stark W (2006) J Am Ceram Soc 892:970
54. Kleinlogel C, Gauckler LJ (2001) Adv Mater 13:1081
55. Zhitomirsky I, Petric A (1999) Mat Lett 40:263